A framework for the estimation of uncertainties and spectral error correlation in Sentinel-2 Level-2A data products

Javier Gorroño, Luis Guanter, Lukas Valentin Graf, Ferran Gascon

Abstract—**The Copernicus Sentinel-2 (S2) satellite mission acquires high spatial resolution optical imagery over land and coastal areas. Delivering uncertainty estimates and spectral error correlation alongside S2 data products facilitates the constrain of retrieval algorithms, propagates further downstream the retrieval uncertainty, and finally makes informed decisions to end-users. This study presents a framework to produce uncertainty estimates and spectral error correlation associated to the S2 L2A data products (i.e. surface reflectance). This framework has been implemented in a prototype code available at [1]. The uncertainty considers both the Level-1 (L1) uncertainty estimates for top-of-atmosphere (TOA) reflectance factor and the atmospheric correction. The L2A error distribution cannot be systematically described as a normal distribution, the transformation can be non-linear and without an explicit mathematical model. Thus, a Multivariate MonteCarlo model (MCM) rather than the law of propagation of uncertainty (LPU) is selected for uncertainty propagation. We show results for surface reflectance uncertainty over the Amazon forest and Libya4 desert site. It illustrates the large uncertainty and spectral error correlation variations depending on the scene. The comparison of an multivariate MCM against an LPU propagation methodology indicate the limitations of the latter for scenes dominated by the atmospheric path. Its implementation as an operational per-pixel processing and dissemination of both the uncertainty and spectral error correlation becomes challenging. Therefore, this methodology is not expected to run at an operational level but serve as the basis to define a strategy for an operational one.**

Index Terms—**Copernicus, uncertainty, spectral error correlation, surface reflectance, Level-2A.**

I. INTRODUCTION

EARTH Observation (EO) via satellite remote sensing has exponentially increased in terms of data and applications in the last decade. It is nowadays an important source of information about the Earth system with areas of application that include, for example, climate studies or agriculture monitoring. The increased complexity of these applications and constantly increasing number of data products has triggered the need to include a quality indicator that describes the compatibility between satellite products and

J. Gorroño is with the Research Institute of Water and Environmental Engineering (IIAMA) at Universitat Politècnica de València

L. Guanter is with the Research Institute of Water and Environmental Engineering (IIAMA) at Universitat Politècnica de València and Environmental Defense Fund

L. V. Graf is with the Crop Science group from the Institute of Agricultural Science at ETH Zurich and the Earth Observation of Agroecosystems Team from the Division of Agroecology and Environment at Agroscope

F. Gascon is with the European Space Agency

the suitability for particular applications. Some initiatives such as Quality Assurance framework for Earth Observation (QA4EO) or FIDUCEO (Fidelity and uncertainty in climate data records from Earth Observations), actively work on a high level framework that becomes the basis of a rigorous quality assessment for EO satellite missions [2], [3].

Recent efforts by the community have made possible for some satellite missions to offer operational Level-1 (L1) uncertainty estimates at top-of-atmosphere (TOA) radiance/reflectance factor. The Moderate Resolution Imaging Spectroradiometer (MODIS) instrument on-board the Aqua and Terra missions produces uncertainty estimates associated with the L1B product [4], [5] as well as the Copernicus Sentinel-2 (S2) satellite mission does it for the L1C products through the L1 Radiometric Uncertainty Tool (L1-RUT) [6]. The Copernicus Sentinel-3 mission also delivers a detailed uncertainty information for the L1B products. They are included at a pixel level for both the Sea and Land Surface Temperature Radiometer (SLSTR) instrument [7] and the Ocean and Land Colour Instrument (OLCI) [8] instruments.

The Copernicus S2 satellite mission currently comprises two satellites (S2A and S2B) and provides continuous monitoring of terrestrial surfaces and coastal waters at a global scale with better than a 5-day revisit [9]. It carries the Multi-Spectral Instrument (MSI) with 13 spectral bands in the visible and near-infrared (VNIR) and the shortwave infrared (SWIR) at spatial resolutions from 10 to 60 m. The S2 Level-2A (L2A) data product is generated after the atmospheric correction of the L1C observations. The L2A product data approximates to the hemispherical–directional reflectance at a surface (or top of canopy level) [10], [11]. From here on, we refer as *surface reflectance* for simplification. The L2A data products are delivered in a set of ortho-images in Universal Transverse Mercator (UTM) projection of about 100 ×100 km [12]. The L2A product represents the most advanced data offered to the users and it is the input to many different land surface parameters such as leaf area index (LAI), the fractional vegetation cover (FVC), and the fraction of absorbed photosynthetically active radiation (FAPAR) in [13]. Including uncertainty information associated to these data products would be highly relevant to improve retrieval algorithms or provide uncertainty information in different end-user applications such as phenology metrics.

Several efforts have been made in bringing uncertainties into land surface parameter retrievals. For example, in [14] where an uncertainty estimate is associated to the LAI, FVC

and FAPAR. The uncertainty is quantified as a combination of the predictive standard deviation and the propagation of the Bi-Directional Reflectance Function (BRDF) model uncertainty. Addtionally, the C3S LAI and FAPAR v4 products [15] include the possibility to manage the whole covariance information at the input Bi-Hemispheric Reflectance (BHR) and propagate to the output results (LAI and FAPAR) [16].

Although these examples represent a clear advance in providing uncertainty estimates in a rigorous manner for land surface parameters, limited detailed uncertainty and covariance information in the observations hinders further efforts. Indeed, it illustrates how the absence of operational uncertainty estimates for surface reflectance products, limits its propagation to further processing levels mainly in land retrieval methods. Thus, the main objective of this project is the generation of uncertainty and spectral error correlation information (i.e. full covariance matrix) associated to the S2 L2A data products.

The impact of this novel information is not only addressed to land surface parameters. It is also expected (but not limited) to:

- *Derive new and better-quality metrics for end-user applications*. For example, in the field of agricultural monitoring, the study in [17] explores an uncertainty propagation framework for the S2 data products that translates the L1C and L2A uncertainty into an uncertainty in the vegetation parameters and ultimately into land surface phenological metrics.
- *Constrain measurement space in retrieval methods*. For example, in optimal estimation methods, the accurate definition of the observation covariance matrix can better constrain the predictions [18].
- *Improve the compliance and quality information of L2A data products*. Reliable information of quantitative EO data products are crucial for decision making processes such as regulatory initiatives or contractual negotiations for the operational exploitation of EO data. [19].

The paper briefly defines the atmospheric correction of the L2A data products in subsection II-A then it describes each one of the considered uncertainty contributions in subsection II-B. The multivariate Monte Carlo method (MCM) is synthesised in subsection II-C. An alternative hybrid version of the law of propagation of uncertainty (LPU) has been implemented and is described in subsection II-D. The results in section III include examples for a scene of the Amazon forest and another in the Sahara desert in subsection III-A. Finally, the difference between a LPU approach and a MCM method are presented in subsection III-B.

II. METHODOLOGY

A. Atmospheric correction in Sen2Cor

The current L2A operational products delivered by the European Space Agency (ESA) are generated with Sen2Cor both from the user side and from the ground segment [20]. Sen2Cor performs a pre-processing of L1C reflectance including a scene classification, an atmospheric correction and a conversion into surface reflectance orthoimages that define the main content of the L2A product. In addition, the algorithm also delivers an

Aerosol Optical Thickness (AOT) map, a Water Vapour (WV) map and a Scene Classification map.

The atmospheric correction is based on precompiled Look-Up tables (LUTs) that contain the main atmospheric functions for a large homogeneous Lambertian surface generated with the Library for Radiative Transfer (LibRadtran) [21], [22].

The input for the Sen2Cor atmospheric correction is the TOA radiance L_{TOA} that is converted from the L1C TOA reflectance ρ_{TOA} for a pixel in the column i and row j as follows:

$$L_{TOA}(i,j) = \frac{E_S \cdot \cos \Theta_s}{\pi \cdot d^2} \rho_{TOA}(i,j) \quad (1)$$

where Θ_s refers to the sun zenith angle (SZA), d to the Sun-Earth distance in astronomical units and E_S refers to the sun irradiance that for the S2 data products is modelled based on Thuillier model [23].

The L2A atmospheric correction algorithm is based on ATCOR$^©$ [24]. Over a flat terrain it neglects, in a first step, the influence of the neighbourhood (adjacency effect) and the surface reflectance is obtained as:

$$\rho^I(i,j) = \frac{\pi \cdot (L_{TOA}(i,j) - L_p)}{\tau \cdot E_g} \quad (2)$$

where τ is the ground-to-sensor transmittance, L_p refers to the path radiance (i.e. solar radiation reflected back to space by the atmosphere before reaching the surface) and E_g to the downwelling irradiance on the ground.

In a second step, the initial surface reflectance is corrected for the adjacency effect following the expression:

$$\rho^{II}(i,j) = \rho^I(i,j) + q \cdot (\overline{\rho^I} - \rho(i,j)) \quad (3)$$

where $\overline{\rho^I}$ represents a mean reflectance of the pixels over a selected range of the adjacency effect and $q = \frac{\tau_{diff}}{\tau_{dir}}$ represents the strength of the adjacency effect. It is the ratio of the diffuse to direct ground-to-sensor transmittance.

The spherical albedo of the atmosphere s on the global flux of the surface needs to be considered. The initial surface reflectance is set to 0.15 for all the spectral bands and needs to be adapted to the scene specific level [24]. Sen2Cor does not include this correction because it is generally negligible. However, we have modelled this step in the prototype implementation so that it can be tested for specific scenarios where it might have a larger impact. The correction is written as:

$$\rho^{III}(i,j) = \rho^{II}(i,j) \cdot [1 - (\overline{\rho^I} - \rho_r) \cdot s] \quad (4)$$

where ρ_r is the reference reflectance set at a value of 0.15.

B. L2A product uncertainty: tree diagram and uncertainty sources

The first step in our analysis involves the definition of the main processing steps and equations for the generation of L2A products (see section II-A).

From here, we can identify the potential sources of uncertainty that stem out of each one of the processing steps. The result of this analysis can be synthesised in an uncertainty tree diagram [3] and is presented in Figure 1.

The tree diagram includes the processing from the L1C products and the different steps presented in section II-A.
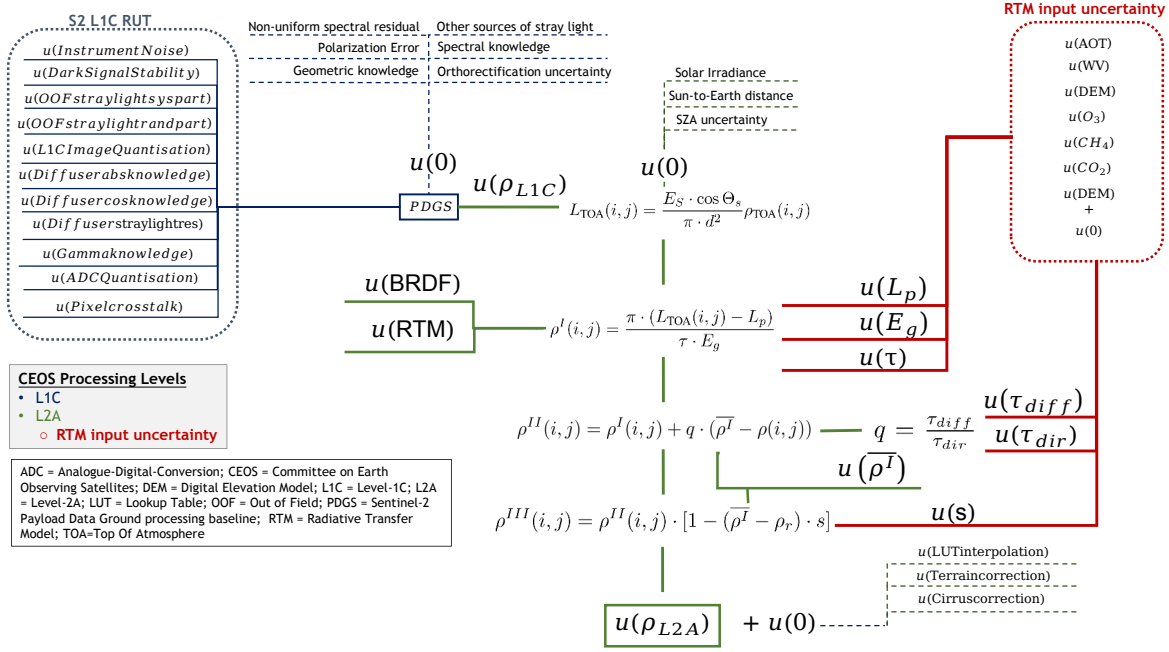
Fig. 1. Uncertainty tree diagram for the S2 L2A products considering the flat terrain case.

Here, the term *u(0)* represents assumptions and approximations that have been identified and are not evaluated. The rest of identified sources of uncertainties are described in the following subsections.

1) L1C uncertainty: The L1C uncertainty is described in [6] and includes several contributions such as the diffuser calibration uncertainty or the dark signal stability.

The original code (available online at https://github.com/senbox-org/snap-rut) has been converted into a sampling scheme based on a MCM methodology. The code considers the spectral error correlation between the considered L1C uncertainty contributions based on the description in [25]. The result is a set of samples for each band that represent the error distribution at L1C reflectance and inherently include the spectral error correlation between them.

The irradiance uncertainty has been also included in the code but only for test purposes. This contribution is cancelled out when considering TOA reflectance uncertainty [6]. However, the data in Sen2Cor is converted back into TOA radiance (see Equation 1) and, although it is cancelled out again during the atmospheric correction, it is possible that a small effect remains and/or other effects (e.g. rounding) need to be considered. Uncertainty for this contribution has been modelled based on estimates in VNIR from [26] and SWIR from [23]. Correlation information has been based on the assumption that the error correlation decreases with the spectral distance.

2) Uncertainty in atmospheric parameters: RTM input uncertainty: The input to the radiative transfer code is a set of parameters (e.g. molecular profile, trace gases, aerosol distribution...) that define the atmospheric model. Then, this model is converted in a set of optical properties (optical depth, single scattering albedo, phase function and boundary

conditions) that solve the radiative transfer equation [21], [22]. The specific solver is that of Discrete-Ordinate-Method Radiative Transfer (DISORT) [27] and the full model description is presented in [28]. In the implementation presented here (see subsections II-C and II-D) we opted for a Multivariate MonteCarlo propagation through DISORT. Despite a detailed mathematical model, it becomes very complex to consider mathematical approximations, rounding values or internal convolution and regridding in Libradtran. Thus, uncertainty on the input atmospheric parameterisation is propagated through the solver and results in an uncertainty on the different atmospheric functions τ, L_p, E_g and s (see section II-A).

Here we detail each one of the main parameters that are included and how they have been parameterised together with the associated uncertainty estimate:

- **Aerosol Optical Thickness** calculated based on the dark dense vegetation (DDV) algorithm in [29] and AOT meteorological estimates from European Centre for Medium-Range Weather Forecasts (ECMWF) CAMS data as a fallback solution [30].
  The theoretical uncertainty for the former becomes highly challenging (e.g. assumed ratios for the bands and correlation). Thus, for this prototype version, the values of uncertainty have been obtained from a diagnostic uncertainty based on the mission requirement and the AOT independent validation.
  On the one hand, the uncertainty requirement for the AOT is modelled as:

$$\sigma_{AOT}^{requirement} = 0.1 \cdot aot + 0.03 \quad (5)$$

  On the other hand, the extensive validation against AERONET stations worldwide has found systematic

underestimation of the AOT value for both DDV and CAMS estimates [31].

Following the recommendations of the GUM [32] for uncorrected systematic errors, we have modelled the total AOT uncertainty as a sum of the requirement uncertainty $\sigma_{AOT}^{requirement}$ and the systematic error obtained from the validation as follows:

$$\sigma_{AOT}^{DDV} = \sigma_{AOT}^{requirement} + |-0.56 \cdot aot + 0.07| \quad (6)$$

$$\sigma_{AOT}^{CAMS} = \sigma_{AOT}^{requirement} + |-0.46 \cdot aot + 0.09| \quad (7)$$

- **Water vapour** This is based on the APDA (atmospheric precorrected differential absorption) algorithm [33]. Same reasoning as for the AOT case applies here and the assigned uncertainty is based again on the requirement values expanded with the systematic error obtained from the AERONET validation as follows:

$$\sigma_{WV}^{requirement} = 0.1 \cdot wv + 0.2 \quad (8)$$

$$\sigma_{WV}^{APDA} = \sigma_{WV}^{requirement} + |-0.1 \cdot wv + 0.03| \quad (9)$$

- **Ozone** is set to 3% based on a comparison from total column ozone (TCO) satellite estimations against ECMWF ERA-interim (currently superseded by ECMWF ERA-5) in [34].
- **SZA, RAA, VZA** uncertainty assumed negligible compared to other sources of uncertainty (e.g. LUT sampling).
- **CH4, CO2 and altitude** assigned a mean of 1.8ppm, 400ppm and mean-tile value from the metadata respectively. Standard deviation allocations of 0.1ppm, 40ppm and 10% respectively.

3) Adjacency correction uncertainty: $u(\overline{\rho^I})$: The adjacency effect is produced by radiation coming from neighbourhood pixels and scattered into the line-of-sight of the sensor. The standard adjacency kernel window size is 2 km. This adjacency range is not a critical parameter for most pixels but for areas with a high surface contrast (e.g a lake surrounded by forests) [20]. However, the simplified modelling of this parameter reduces the processing time but might not capture the spatial dependence of the adjacency effect. For example, more complex definitions as in ATCOR include a range dependent weighting [24].

For this first implementation of the L2A budget, the term $\overline{\rho^I}$ in Equation 3 has been modelled with an uncertainty of 3% and a spectral error correlation based on the spectral distance.

4) Lambertian assumption error: $u(BRDF)$: The retrieval presented in subsection II-A assumes a Lambertian surface. However, in a real scenario the target surface is expected to be anisotropic and this results in an error on the estimated surface reflectance. These errors depend on the specific target and spectral band. For example, relative errors due to the Lambertian assumption on the surface reflectance have been calculated as 3–12% in the visible and 0.7–5.0% in the near-infrared in [35]. In another example in [36], mean errors where 3–7% in the red and 2–5% in the near-infrared (depending on optical depth).

For this implementation, we set an uncertainty of 3% for all bands. It might be slightly optimistic for some visible bands but average case in NIR bands.

5) LibRadtran uncertainty $u(RTM)$: This last contribution represents the uncertainty introduced by the radiative transfer itself. Benchmarking of radiative transfer typically relies on the comparison of ideal cases such as monochromatic radiation or Lambertian surface assumptions [37]. Although this might be a good initial assessment to validate and flag issues between radiative transfer codes, it does not represent real conditions for EO satellite observations.

Recent work in [38] considers pseudo-invariant sites to infer uncertainty in radiative transfers with a data-driven method. The study in [39] also presents specific radiative transfer model (RTM) disagreements over pseudo-calibration sites. This second study provides detailed results for different codes (among them Libradtran) and for the Sentinel 2 satellite mission. This per-band errors are calculated as the maximum disagreements between mean bias errors over a long temporal trend of S2 satellite observation against simulated scenes over the Libya-4 calibration site. Although it covers a single site, they are the most detailed and S2-specific estimates of inherent Libradtran uncertainty and we have included them in the first version of the L2A uncertainty. In the VNIR bands, the estimated errors are from 1-2%. The largest relative error is reported for B11 and B12 at the 2-3% where the absorption parameterisation (in this case the REPTRAN model available for S2 in Libradtran [40]) has limited capability to reproduce the varying molecular absorption. The error for B8 is reported above 3% but here we will reduce the error to 1.2% since a large contribution was due to the limited spectral resolution of 6SV (see [41]) that is not present in Libradtran.

C. Multivariate Monte-Carlo methodology

The most common approach for uncertainty estimation is referred as *Guide to the expression of uncertainty in measurement* (GUM) and involves the analytical calculation of the uncertainty through partial derivatives and correlation coefficient [32]. That is, the law of propagation of uncertainty (LPU). The LPU was the selected methodology for the S2 L1C uncertainty since the expected radiometric transformations are largely linear and a normal error distribution can be assumed for the output measurand [6].

The L2A data products from S2 are generated with Sen2Cor processor [42]. It is based on the retrieval of the surface reflectance based on atmospheric functions precalculated with Libradtran.

The RTM converts the parameterisation of the atmosphere model (e.g. AOT, height...) into an optical model that solves the radiative transfer equation. Although the RTM can be defined by a set of equations [21], its mathematical description is limited. For example, the majority of radiative transfer codes, include numerical integration and other approximations that results in a very complex mathematical formulation [43]. When considering an entire radiative transfer code, this becomes even more complex since it might involve an internal convolution of the atmospheric transmittance or other effects such as rounding values [28].

In general, we find no explicit mathematical model of the atmospheric functions, no knowledge of their distribution shape,

dependence or linearity of the model. In that scenario, the MonteCarlo Model (MCM) is the selected choice since it can work without an explicit mathematical model and can model the input and output dependence and distribution shape [44].

The Monte Carlo method is based on three different steps:

- The assignment of probability distributions to the input quantities as defined in subsection II-B. All inputs, included L1C data, are modelled with a spectral error correlation matrix as well as an uncertainty per band.
- We extract samples from the input quantities and calculate the processing steps as defined in subsection II-A. It involves the run of Libradtran to generate the error distribution associated to each one of the atmospheric functions [21], [22] and the calculation of equations 2, 3 and 4 to obtain the surface reflectance.
- The previous steps are repeated in an iterative manner. The output represents an error distribution (with implicit error correlation between S2 bands) where the measurand (here the surface reflectance) is contained [45]. Here we offer the uncertainty (k=1) based on the standard deviation of the surface reflectance samples in a normal distribution. If the distribution is considerably asymmetric, the reference [45] recommends the use of the shortest coverage interval that corresponds to a specific coverage factor (e.g. 68.27% for k=1).

This method has been implemented in a software version and is accessible in [1].

D. Law of propagation of uncertainty

As mentioned previously, it is rather complex to model a mathematical expression of the RTM. However, the combination of the atmospheric functions has been described in Equations 2, 3 and 4. Thus, here we propose an alternative method that combines a MCM method to estimate the probability distribution of the atmospheric functions and the LPU methodology for their combination.

The same software in [1] provides the distribution for each one of the atmospheric functions L_p, E_g, τ and s. Then, a corresponding value of uncertainty can be obtained for each atmospheric function as well as the correlation among them. Furthermore, the sensitivity coefficient for each atmospheric function can be defined from the defined Equations 2, 3 and 4.

In mathematical terms, the LPU framework is defined in matrix form as:

$$U = C \times V \times R \times V^T \times C^T \qquad (10)$$

Here C represents the diagonal matrix of the sensitivity coefficients where the non-zero entries are defined as:

$$\mathbf{C}[i,i] = \begin{bmatrix} \frac{\partial \rho_{L2A}}{\partial L_{TOA}} & -\frac{\partial \rho_{L2A}}{\partial L_{TOA}} & \frac{\partial \rho_{L2A}}{\partial \tau} & \frac{\partial \rho_{L2A}}{\partial E_g} & \frac{\partial \rho_{L2A}}{\partial s} \end{bmatrix} \qquad (11)$$

and V a diagonal matrix with the non-zero entries defining the individual uncertainty sources corresponding to the atmospheric functions and the L1C radiance as follows:

$$\mathbf{V}[i,i] = \begin{bmatrix} \sigma(L_{TOA}) & \sigma(L_{path}) & \sigma(\tau) & \sigma(E_g) & \sigma(s) \end{bmatrix} \qquad (12)$$

The R matrix is the error correlation matrix between the individual uncertainty sources. On the top of this uncertainty, an effect related to adjacency or other effects might be added.

This analytical and matrix implementation of the uncertainty is an efficient method for integration in the Sen2Cor processor since it minimises the computational requirements on the user side by pre-compiling the uncertainty values for each atmospheric function and correlation. These values could be stored alongside each one of the LUT entries of Sen2Cor. That is for each specific LUT entry in Sen2Cor, we would have the values, uncertainty and error correlation between the atmospheric functions.

We will use this method to compare against the proposed MCM multivariate in subsection III-B in order to flag the main strengths and limitations.

III. RESULTS

A. MCM results over two scenes

This subsection exemplifies a run and output of the software over two selected sites. These sites are located at the latitude and longitude -6.2869°, -66.8652° and 28.55°, 23.39°. They represent a typical Amazon forest and dune area of the Sahara desert. The latter is largely used by the community for radiometric validation of optical instruments onboard satellites [46]. The area selected for both sites is 500×500 m². Figure 2 contains an RGB image for each one of the sites.

The error distributions for the TOA radiance results in a near-normal distribution as expected [6]. The relative uncertainty varies from 1 to 3% mostly depending on the radiance level. Figure 3 contains the error distribution for a subset of bands of the surface reflectance that we have obtained by running the multivariate MCM code with 4000 samples. The mean and standard deviation for all the S2 L2A bands are included in Table I.

The relative uncertainty here varies largely depending on the band. The larger relative uncertainty occurs for B9 due to large sensitivity to water vapour. The lowest relative uncertainty (in the range of 3-5%) occur for the rest of the bands in the NIR and SWIR. However, these relative values increase for those bands that are more sensitive to the atmosphere (e.g. B1-B4). In those bands, the values can range from 5% to values over the 20%. The error distributions at surface reflectance follows a normal distribution for several bands. This situation does not occur for B9 and B1-B4 of the Amazon forest example. The non-normal distribution of B9 is the result of a large impact of the water vapour absorption and its non-linear response. The slight skewness in the B1-B4 distribution is due to higher impact of the atmosphere.

Figure 3 is the result of combining different atmospheric functions and the additional correction steps (see subsection II-B). These atmospheric functions are presented in Figure 4 for the bands B1 and B9.

The distribution of the different atmospheric functions are close to normal for the desert example, supporting the surface reflectance results. In contrast, the distribution for the different atmospheric functions in the Amazon forest case are highly non-normal and irregular. For some functions but mainly for

TABLE I
SURFACE REFLECTANCE MEAN AND STANDARD DEVIATION OF THE S2 L2A BANDS FOR AMAZON AND LIBYA-4 CASES

Amazon	B1	B2	B3	B4	B5	B6	B7	B8	B8A	B9	B11	B12
Mean	0.039	0.038	0.050	0.029	0.078	0.232	0.297	0.319	0.341	0.535	0.148	0.056
Std[%]	24.72	19.39	10.85	13.45	5.70	3.79	3.45	3.36	3.39	41.82	3.92	4.60
Libya-4	B1	B2	B3	B4	B5	B6	B7	B8	B8A	B9	B11	B12
Mean	0.166	0.227	0.341	0.483	0.525	0.535	0.564	0.586	0.590	0.747	0.734	0.694
Std[%]	9.32	5.95	4.13	3.49	3.77	3.56	3.35	3.32	3.35	31.5	3.55	3.57

(a) Amazon Forest
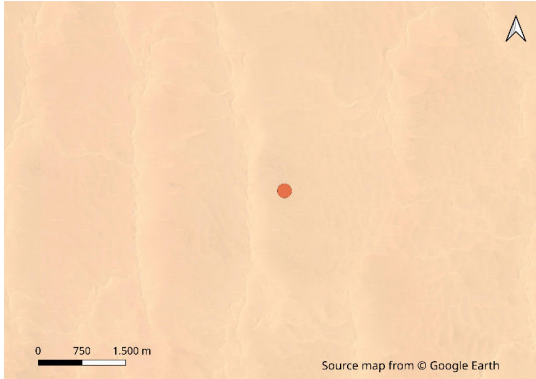
(b) Libya-4 desert

Fig. 2. Selected sites with Figure 2a containing the Amazon forest centered at the latitude and longitude -6.2869°, -66.8652°and Figure 2b) containing the Libya4 desert at the latitude and longitude 28.55°, 23.39°(a) Amazon Forest. (b) Libya-4 desert.

the downwelling irradiance E_g, the distribution presents some clipping. This can be attributed to the input AOT distribution that for the Amazon fores is set to a mean of 0.07 and standard deviation of 0.68 (see Equation 6). Thus, part of the input AOT has been clipped to zero. On the contrary, the AOT for Libya-4 is 0.21 with a standard deviation of 0.1 that results in a small number of clipped values. In general, larger clipping occurs for AOT values below 0.1 where the sytematic uncertainty represents a floor value that rapidly scale in relative terms. This is realistic (i.e. a certain part of the uncertainty budget does not scale with the AOT value) but represents a challenge in the distribution modelling.

Despite larger irregular patterns in the distribution of the atmospheric functions, the results in the distribution at the surface reflectance only partially reflect a small non-normal response. That is, at some extent, due to the combination of

the atmospheric functions these effects are cancelled out. For example, the down-welling direct (E_g^{dir}) and diffuse (E_g^{diff}) are completely inversely correlated (i.e. opposite distribution shapes).

In addition to the information of the specific per-band uncertainty, the software also generates the error correlation matrix between the S2 bands. The result for each one of the examples is given in Figure 5.

At a first glance, it is clear that the spectral error correlation is very different for the two sites. The Amazon example shows a strong correlation between B1-B4 bands and B6-B8A bands separately. These bands correspond to those dominated by the atmosphere and the surface signal respectively. The error correlation for the desert case are significantly higher as a consequence of a much higher surface reflectance. The correlation tends to decrease with the spectral distance except in the case of B9. In that case, the band is uncorrelated with most of the bands except for those that have a minor sensitivity to water vapour.

B. LPU vs. MCM multivariate approach

Subsection II-D described the methodology to obtain uncertainty estimates with a LPU methodology for the combination of the atmospheric functions. It was anticipated the expected complexity of using this approach due to the non-linear response and ad-hoc solutions of the radiative transfer code.

This subsection implements the same examples as in subsection III-A but using both the LPU framework and MCM multivariate approach. The comparison only considers the propagation of the RTM input uncertainty and L1C uncertainty (see Figure 1). That is, the combination described by Equation 2. Further uncertainty sources related to the adjacency correction, the Lambertain assumption of the correction model and the estimated accuracy of the LibRadTran software are not included. These have been modelled as a normal distribution in the absence of further information. Thus, not including these sources, facilitates the identification of disagreements in the intercomparison.

Table II presents the surface reflectance uncertainty differences between the LPUC and MCM combination for all L2A bands.

There is a high level of agreement for all bands except for those most affected by AOT (B1, B2 and B3) and water vapour (B9) where disagreements between a LPU approach and MCM multivariate appear.

We have produced another example analogue to the one presented here but Libradtran has been parameterised with a water vapour level of 5 cm and AOT of 1.14 (approximately 5
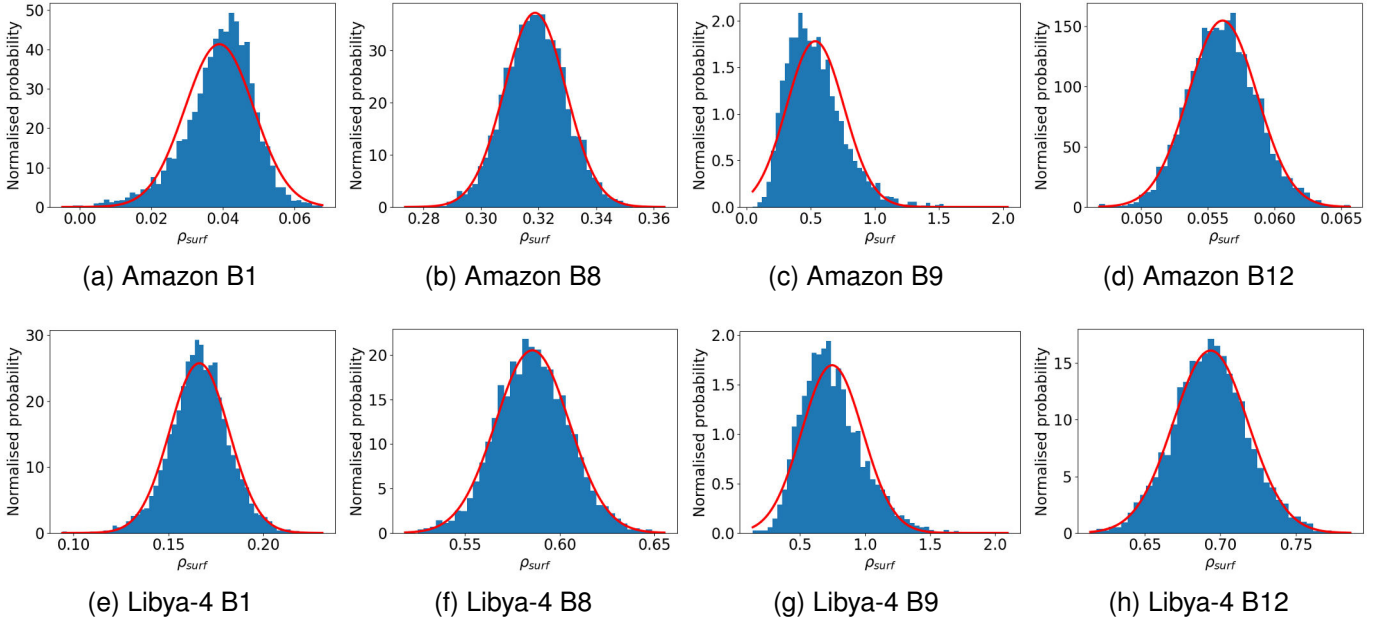
Fig. 3. Surface reflectance distribution obtained with the L2A-RUT code for bands B1, B8, B9 and B12 and the Amazon and Libya-4 sites described in Figure 2. The red line corresponds to the ideal normal fitting.

TABLE II
L2A UNCERTAINTY FOR AMAZON AND LIBYA-4 CASES USING AN MCM APPROACH AND LPU METHODOLOGY FOR THE COMBINATION OF THE ATMOSPHERIC FUNCTIONS. THE ADJACENCY CORRECTION, THE LAMBERTAIN ASSUMPTION OF THE CORRECTION MODEL AND THE ESTIMATED ACCURACY OF THE LIBRADTRAN SOFTWARE ARE NOT INCLUDED.

Amazon	B1	B2	B3	B4	B5	B6	B7	B8	B8A	B9	B11	B12
Std LPU[%]	12.61	11.20	6.59	8.72	3.67	1.93	1.47	1.34	1.67	31.07	1.91	3.13
Std MCM[%]	10.81	9.75	5.34	7.77	3.38	1.91	1.19	1.12	1.50	42.51	1.89	3.30
Libya-4	B1	B2	B3	B4	B5	B6	B7	B8	B8A	B9	B11	B12
Std LPU[%]	3.85	2.79	1.90	1.45	1.72	1.52	1.30	1.21	1.43	23.78	1.19	1.48
Std MCM[%]	1.56	1.46	1.26	1.24	1.97	1.57	1.22	1.16	1.38	30.60	1.26	1.71

km visibility). This represents an extreme but realistic scenario since they correspond to the highest values stored in the pre-compiled LUT of Sen2Cor. Figures 6 presents the surface reflectance distribution for a set of L2A bands

The distribution for almost all the cases are highly non-normal and disagree with a LPU framework. Thus, these examples indicate that the LPU approach is not valid when the atmosphere dominates over the surface signal. Figure 6a has a positive mean value of 0.039 but includes a fraction of the distribution in negative values as a result of an overcorrection of the atmosphere.

We have further extended the intercomparison to map LPU and MCM multivariate results as a function of both AOT and WV values. Figure 7 presents the uncertainty map as a function of AOT and WV values for the Amazon site (see Figure 2a) and B8. The calculation points for AOT are from 0 to 1 in 0.25 steps and WV gridding from 0 to 6 cm in 1.5 cm steps. A version in a reduced range is also calculated with AOT values from 0 to 0.3 in 0.05 steps and WV from 0 to 3 cm in 0.5 cm steps. The MCM uncertainty has been calculated with 500 samples for each run and two different methodologies. First as a standard deviation of the error distribution (MCM std.) and then, as the 68.27% of probability around the median value

(MCM unc.).

The results for B8 shows generally large differences. These differences are significant for large values of WV where the LPU tends to overestimate the uncertainty. Observing the surface reflectance distribution in Figure 6b, it is visible that the small sensitivity of B8 to water vapour absorption results in a highly peaked distribution that leads to an overestimation of the LPU approach. There are also small differences between the MCM std. and MCM unc. The small overestimation of the MCM std. with high water vapour that can be associated to the right skewness of the distribution in Figure 6b.

IV. DISCUSSION

A. Main findings

The subsection III-A presents two examples (one for the Amazon forest and the other for Sahara dune desert) that were useful to test the code and examine the first results.

The first interesting point is that, in comparison to the L1C uncertainty estimates, the L2A uncertainty estimates are larger in relative terms and present a larger spectral band dependence. That is, the range of relative uncertainty at L1C moves from 1 to 3% for the examples and 3-20% for the L2A uncertainty estimates. The atmospheric correction increases the relative
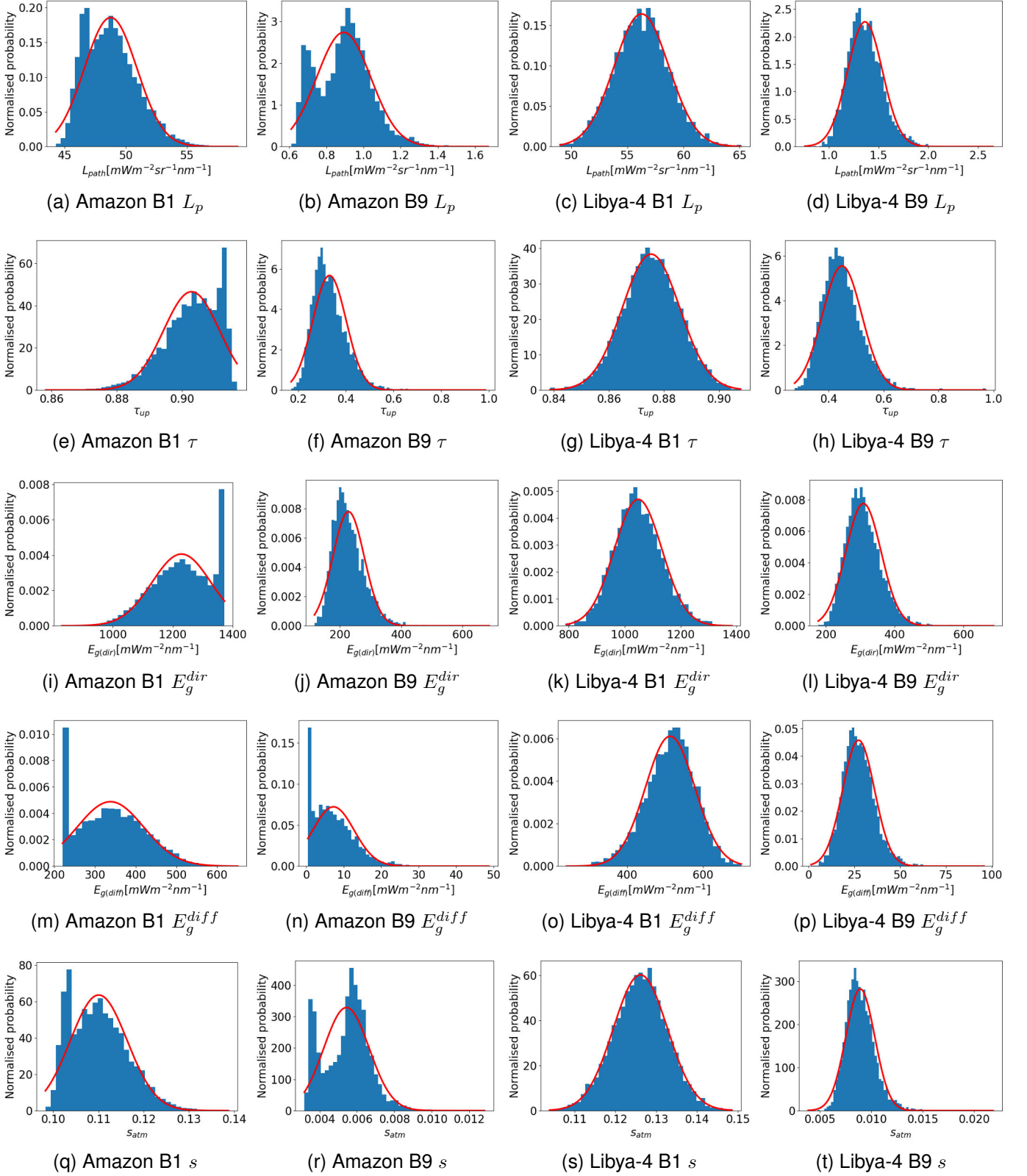
Fig. 4. Atmospheric function distribution (L_p , τ ,E_g^{dir},E_g^{diff} and s) obtained with the L2A-RUT code for bands B1 and B9 and the Amazon and Libya-4 sites described in Figure 2. The red line corresponds to the ideal normal fitting.

uncertainty by reducing the available signal and by introducing an uncertainty associated to the correction. For those bands

with little impact of the atmosphere, the surface reflectance distribution is largely normal. However, this is not the case
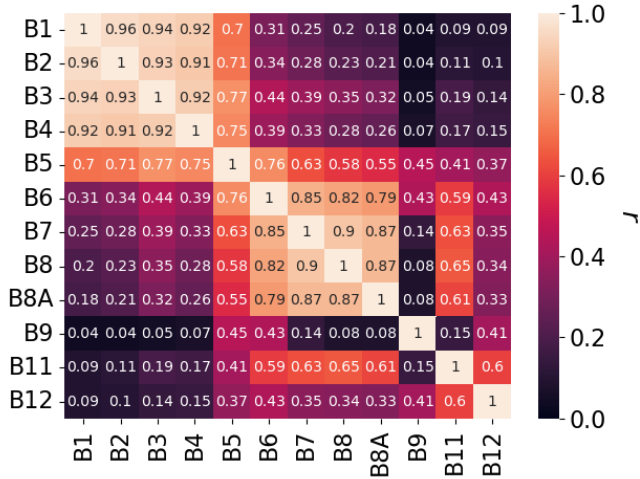
(a) Amazon spectral error correlation
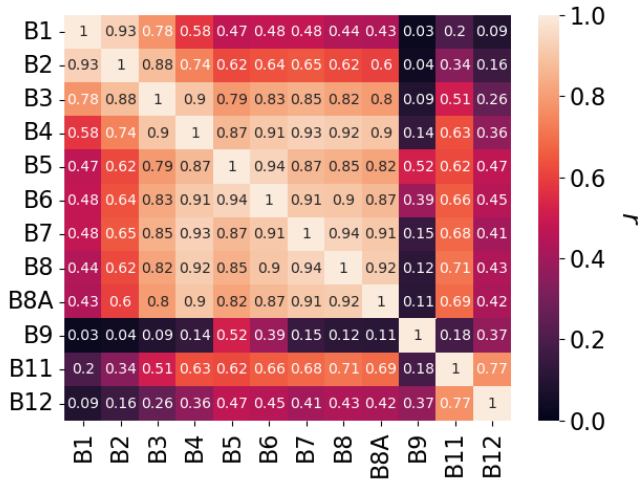
(b) Libya4 spectral error correlation

Fig. 5. S2 L2A spectral error correlation for Amazon site (Figure 5a) and desert site (Figure 5b)

for those bands where the atmosphere dominates. For example, the error distribution for B9 is generally non-normal due to its sensitive to water vapour.

The results in subsection III-A illustrate important differences between the two sites not only at uncertainty levels but more importantly on their spectral error correlation. The Amazon example shows a strong correlation between B1-B4 bands and B6-B8A bands separately as a consequence of the vegetation red-edge. The error correlation in the desert case is higher due to the higher surface reflectance with a dependence on the spectral distance.

We also explored in detail the non-normal distribution of the surface reflectance and its implications to calculate the uncertainty using different methodologies. The individual atmospheric functions presented in Figure 4 can indiviually show the non-normal and irregular distribution of each one of them. On the one hand, it shows that the combination of some of these functions (e.g. diffuse and direct irradiance) is partially cancelled when combined. On the other hand, it also

shows the effect of clipping input distributions such as AOT. In that case, it shows that we need to consider more realistic and potentially non-normal distributions of the input sources.

Comparing to a LPU approach (see subsection II-D), the study in subsection III-B has illustrated the limits of assuming normal distributions and linear responses. Setting extreme but possible atmospheric conditions with water vapour level of 5 cm and AOT of 1.14 (approximately 5 km visibility) the results between the two methods largely disagree for all bands. This comparison was refined by producing an uncertainty map as a function of AOT and WV in Figure 7. It shows that the LPU tends to overestimate the uncertainty with an important effect of water vapour in B8. There were also differences between the standard deviation of the output distribution and the direct assessment of the 68.27% of probability around the median.

In general, the LPU method is valid as long as the atmosphere is not dominant and input sources are normally distributed. Any band that is highly sensitive to atmospheric absorption and scattering will be affected. For the S2 satellite mission this occurs for some bands and scenes. That is, the proposed methodology proposed in subsection II-D has a limited application at a global scale. Upcoming Copernicus satellite missions such as CHIME or S2-NG will include a larger and narrower number of bands. It is expected that a more detailed and reviewed multivariate MCM model is needed to assess the uncertainty and its comparison against other alternative approaches.

B. Further work

Although a large number of uncertainty sources are included, some of them are not yet available at this version. Under some scenarios, it is possible that this results in a small underestimation of the current L2A uncertainty levels. However, it is the idea that subsequent versions of this software include refined and/or novel uncertainty sources.

The work in [6] describes the missing contributions for the L1C uncertainty estimates. These are effects such as spectral response, polarisation or orthorectification that depend on the scene. Relevant improvements are on-going to model these contributions. For example, the work in [47] describes the efforts to provide in the upcoming S2 satellite units (C/D) a per-pixel spectral response. The orthorectification of the S2 data products at L1C (TOA reflectance) has been also studied in [48].

The work here presented includes the uncertainty associated to the atmospheric correction that is applied to the S2 L2A data products. The contributions described in subsection II-B include the most relevant effects of this process. However, there are specific corrections that are not considered here. Both the terrain and cirrus correction are included as an option in the Sen2Cor software and should be specifically studied in subsequent revisions. Sen2Cor also contains a LUT with pre-compiled values for the atmospheric functions at different parameterisations. Thus, in a real-scenario the atmospheric functions are interpolated values from the LUT an requires the assessment of the interpolation error. The uncertainty associated to the atmospheric profile and AOT model are also important and challenging contributions to be considered. For the latter,
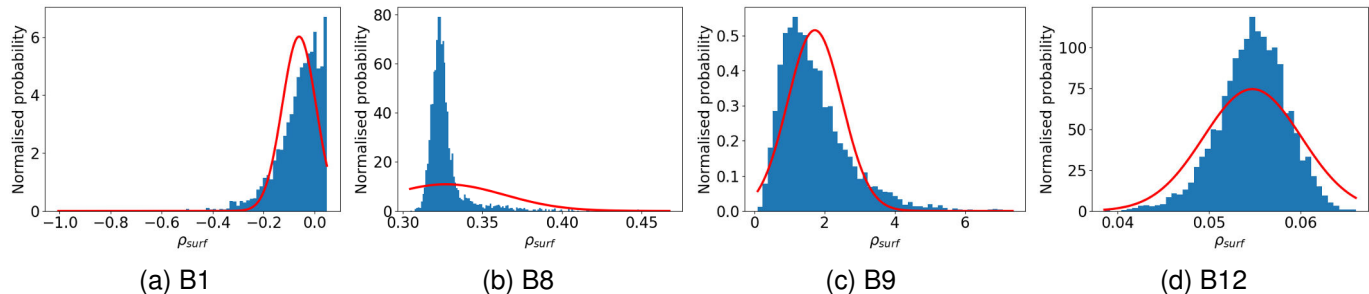
Fig. 6. Surface reflectance for a set of bands in the Amazon case obtained for a uniform lambertian approach (i.e. equation 2) for both the MCM mulitvariate and LPU approach. The simulation was forced to set a value of 5 cm for water vapour and 1.14 (approximately 5 km visibility) for AOT. The red line represents the normal distribution associated to the uncertainty value of the LPU approach.
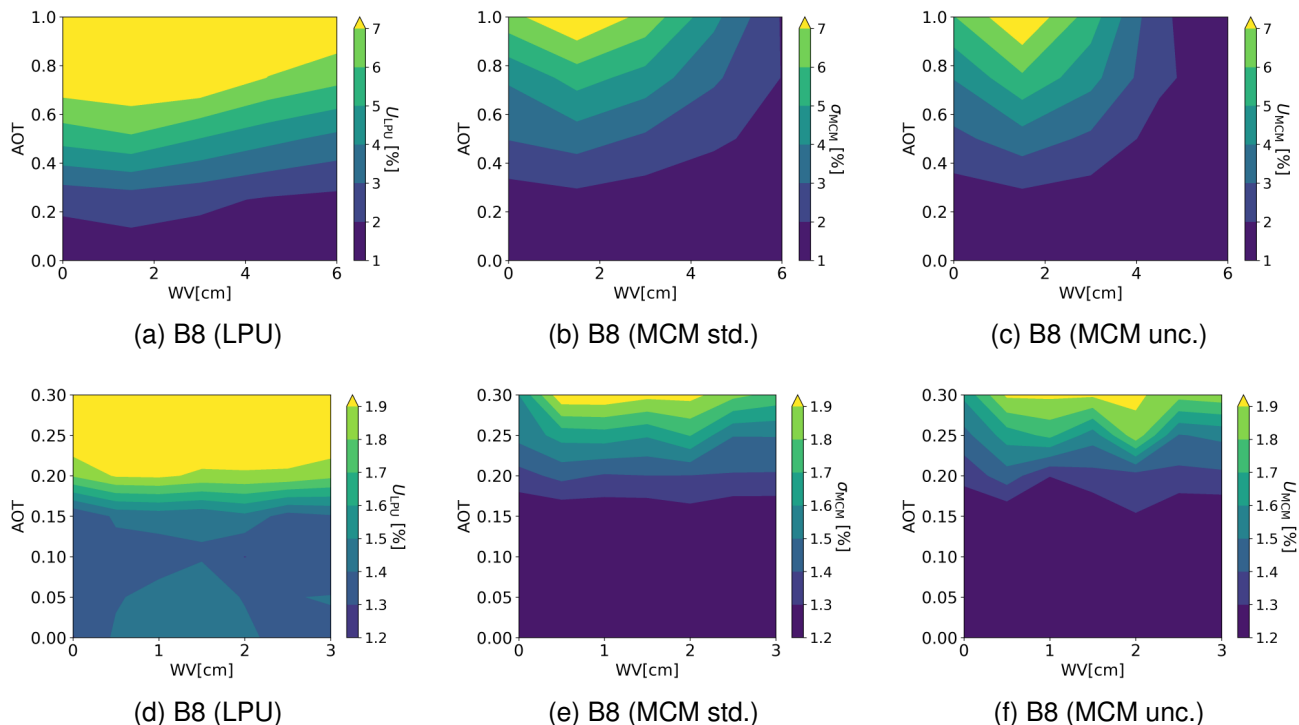
Fig. 7. Map of surface reflectance uncertainty as a function of AOT and WV in the Amazon case obtained for a uniform lambertian approach (i.e. equation 2) for the MCM multivariate and LPU approach and band B8. The former method has been calculated as a standard deviation of the error distribution (MCM std.) and the 68.27% of probability around the median value (MCM unc.). The top three figures have been obtained AOT gridding: 0 to 1 in 0.25 steps and WV gridding from 0 to 6 cm in 1.5 cm steps. The bottom three figures set an AOT gridding from 0 to 0.3 in 0.05 steps and WV from 0 to 3 cm in 0.5 cm steps.

we exemplify its impact on L2A uncertainty estimates and discuss potential implementations in subsection IV-C.

For the uncertainty sources that have been included in this first prototype version, we have included a simplified allocation value in several cases. More importantly is that these input distribution have been assumed Gaussian. The results in subsection III-A show that this might be limited and unrealistic for parameters such as AOT and WV. Furthermore, the proposed uncertainty estimates are highly dominated by the systematic errors obtained during validation [31] (see subsection II-B2). This is a continuous effort and future updates might consider more detailed information such as a per-biome uncertainty. Other uncertainty sources such as the adjacency effect $u(\overline{\rho^I})$ are based on first guess values. In the absence of other information, this is a valid approach. However, subsequent studies should

be dedicated to assess more specific uncertainty estimates for these sources.

Finally, one of the most important novelties in this study is the consideration of spectral error correlation through the entire processing chain. Uncertainty contributions here are assigned spectral error correlation matrices dependent on the spectral distance and the focal plane (VNIR or SWIR). Nonetheless, we are aware that the information available is limited and contributions like *Libradtran uncertainty* and *lambertian assumption* (see subsections II-B5 and II-B4 respectively) have a strong impact on the final budget. In general, the attachment of spectral error correlation information in pre-flight calibration certificates or atmospheric studies should be encouraged in future studies.
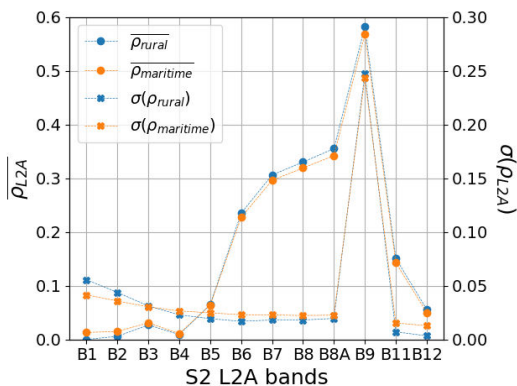
Fig. 8. Mean and standard deviation of the L2A surface reflectance distribution for the Amazon scene with an adjusted AOT value of 0.5 and considering the default rural boundary layer aerosol and maritime type one.

C. Considering the uncertainty on AOT models

Sen2Cor calculates the atmospheric functions based on the Libradtran default aerosol according to [49]. These properties refer to a rural type aerosol in the boundary layer, background aerosol above 2km, spring-summer conditions and a visibility of 50 km. These optical or microphysical settings may be modified in Libradtran [21]. In Sen2Cor user mode, the aerosol profile in the boundary layer can be modified and it is automatically detected by the L2A-RUT code. However, no uncertainty is associated to the default profile expecting to introduce important errors where the AOT is high and profiles differ from the standard case.

To exemplify the impact that the AOT model could have on the estimates, we run the L2A-RUT for the Amazon case with a value of AOT 0.5 with both the rural and maritime boundary layer aerosol as in [49]. The mean and standard deviation for all L2A bands are displayed in Figure 8.

The results indicate important differences both in terms of mean and standard deviation with the maritime model showing higher mean values in the lower wavelenghts and higher values at longer wavelengths (viceversa for the standard deviation). Future versions will require an important effort that is not so much focused on the possibility of modelling the AOT profiles (Libradtran and other RTC are well-suited for this purpose) but rather on associating an uncertainty to a per-pixel case. Potential solutions that could be explored include the association of a potential range of values over specific sites based on aerosol properties climatology (e.g. [50]).

D. Towards an operational version

The current implementation in [1] allows the users to a rapid access to queries for an uncertainty and spectral error correlation assessment of a pixel or set of them. It is an ideal solution for small area studies or a general understanding of the expected L2A uncertainty and spectral correlation over scenes types. However, the proposed multivariate MCM is computationally expensive and the amount of information at a pixel-level becomes prohibitive. Thus, this methodology is not expected to run at an operational level but serve as the basis to explore and validate different strategies for operational implementation.

Using an LPU method is not discarded here but we have seen that its domain of validity is reduced as compared to a similar MCM model. Thus, it could be possible to set up the LPU method but restricting its applicability to valid cases or modify to include higher-order derivatives. Otherwise, consideration should be given to using MCM or alternative approaches [51]. In a way, the implementation of an MCM model as in here is recommended as a validation tool for an LPU or other methodology.

The calculation of the uncertainty and spectral error correlation for a single pixel, area or set of pixels does not constitute a major challenge in terms of data volumes. However, the per-pixel calculation and storage of these data volumes might become unfeasible. Upcoming Copernicus satellite missions such as CHIME or S2-NG [52] will further increase the demand with a larger set of bands and higher spatial resolution. Thus, alternatives must be sought for a global distribution of this information.

In the last years, it is common practice to consider emulators as fast approximations of the atmospheric correction model. We can find already examples such as the one in [53] where they achieved an emulator with an accuracy $<1\%$ (k=2) with respect to MODTRAN radiative transfer. Another example in [54] proposes a surrogate model to generate a candidate result that is refined with an emulator that corrects for the difference between the surrogate model and a complex accurate radiative transfer model. Translating this from atmospheric correction into surface reflectance uncertainty, it could be possible to train such models with an MCM model similarly as the one presented here. Thus, these types of models could be instrumental to deliver not only uncertainty but also spectral error correlation or error distributions at a pixel-level to the users.

An alternative atmospheric correction method is to consider the mapping between TOA observations and surface reflectance with bayesian methods such as optimal estimation method [55]. For example, the work in [56] implemented an atmospheric correction that can be applied to generate S2 L2A products. Compared to a multivariate MCM and a LPU approach (see subsections II-C and II-D), this method has the advantage to directly offer the variance matrix (both uncertainty and spectral error correlation matrix) in the retrieved space. However, the uncertainty propagation in optimal estimation relies on prior data that does not necessarily approximate the real scene such as in the case of extreme events. Furthermore, it also assumes normal distribution, unbiased measurements and moderately linear Jacobian matrix [18].

Thus, a similar cross-comparison as in subsection III-B can be applied to, for example, identify scenarios where the Jacobian of the atmospheric model might not be sufficiently linear. Indeed, it is possible not only to identify but also to adapt these Bayesian frameworks so that these limitations are (partially) overcome. For example, the work in [57] also defines a multivariate MCM sampling of the Bayesian retrieval algorithm so that the retrieved covariance matrix accounts for the model discrepancy.

V. Conclusions

We presented the L2A-RUT software tool (available at [1]) that delivers both uncertainty estimates and spectral error correlation from the S2 L2A data products (i.e. surface reflectance). The methodology considers the uncertainty of the S2 L1C data products and the atmospheric correction. We have set a MCM multivariate model that accounts for the spectral error correlation between S2 L2A bands and propagates the uncertainty of the L1 TOA reflectance, atmospheric parameterisation and adjacency correction. On the top of this propagation we also model the contributions from the Lambertain assumption and the estimated accuracy of the atmospheric radiative transfer. The results over a forest and desert scene illustrate the large variations both in uncertainty levels and spectral error correlation that can be found between data products. The selection of the MCM multivariate model over a LPU scheme is justified because the error distribution cannot be systematically described as a normal distribution, the transformation can be non-linear and the atmospheric correction is not fully described by a mathematical model. An inter-comparison between these two combination models has shown important differences that are dependent on the spectral band, AOT and WV levels. In addition, we observe how the modelling of input distributions (e.g. AOT) as a normal distribution can be limited and unrealistic in the error propagation. The current tool version here presented delivers information to the user for a selected pixel, small area studies or a general estimation of the L2A uncertainty and spectral correlation over scenes types. The multivariate MCM here proposed cannot be extended to process global per-pixel and disseminate both L2A uncertainty and error spectral correlation. Nonetheless, it can be helpful to validate and study different implementation strategies at an operational level so that per-pixel uncertainty and spectral error correlation can be delivered to the users.

Acknowledgments

VI. References Section

References

[1] J. Gorroño, "gorronyo/S2-L2A-RUT: Simple code and parallel improvement," Jun. 2024. [Online]. Available: https://doi.org/10.5281/zenodo.11971517

[2] Q. T. Team, "A quality assurance framework for earth observation: Principles," 2010.

[3] J. Mittaz, C. J. Merchant, and E. R. Woolliams, "Applying principles of metrology to historical earth observations from satellites," *Metrologia*, vol. 56, no. 3, p. 032002, may 2019. [Online]. Available: https://dx.doi.org/10.1088/1681-7575/ab1705

[4] J. A. Esposito, X. Xiong, A. Wu, J. Sun, and W. L. Barnes, "MODIS reflective solar bands uncertainty analysis," in *Earth Observing Systems IX*, W. L. Barnes and J. J. Butler, Eds., vol. 5542, International Society for Optics and Photonics. SPIE, 2004, pp. 448 – 458. [Online]. Available: https://doi.org/10.1117/12.558106

[5] X. Xiong, A. Angal, W. Barnes, H. Chen, V. Chiang, X. Geng, Y. Li, K. Twedt, Z. Wang, T. Wilson, and A. Wu, "Updates of MODIS on-orbit calibration uncertainty assessments," in *Earth Observing Systems XXII*, J. J. Butler, X. J. Xiong, and X. Gu, Eds., vol. 10402, International Society for Optics and Photonics. SPIE, 2017, p. 104020M. [Online]. Available: https://doi.org/10.1117/12.2276305

[6] J. Gorroño, N. Fomferra, M. Peters, F. Gascon, C. I. Underwood, N. P. Fox, G. Kirches, and C. Brockmann, "A radiometric uncertainty tool for the sentinel 2 mission," *Remote Sensing*, vol. 9, no. 2, 2017. [Online]. Available: https://www.mdpi.com/2072-4292/9/2/178

[7] D. Smith, S. E. Hunt, M. Etxaluze, D. Peters, T. Nightingale, J. Mittaz, E. R. Woolliams, and E. Polehampton, "Traceability of the sentinel-3 slstr level-1 infrared radiometric processing," *Remote Sensing*, vol. 13, no. 3, p. 374, Jan. 2021. [Online]. Available: http://dx.doi.org/10.3390/rs13030374

[8] J. S. Fahy and S. E. Hunt, "Uncertainty analysis for sentinel-3 olci radiance observations," in *2021 IEEE International Geoscience and Remote Sensing Symposium IGARSS*, 2021, pp. 8150–8153.

[9] M. Drusch, U. Del Bello, S. Carlier, O. Colin, V. Fernandez, F. Gascon, B. Hoersch, C. Isola, P. Laberinti, P. Martimort, A. Meygret, F. Spoto, O. Sy, F. Marchese, and P. Bargellini, "Sentinel-2: Esa's optical high-resolution mission for gmes operational services," *Remote Sensing of Environment*, vol. 120, pp. 25–36, 2012, the Sentinel Missions - New Opportunities for Science. [Online]. Available: https://www.sciencedirect.com/science/article/pii/S0034425712000636

[10] F. Nicodemus, J. Richmond, J. J. Hsia, I. Ginsberg, and T. Limperis, "Geometrical Considerations and Nomenclature for Reflectance," National Bureau of Standards, U.S. Department of Commerce, Washington, DC, Tech. Rep. October, 1977.

[11] G. Schaepman-Strub, M. E. Schaepman, T. H. Painter, S. Dangel, and J. V. Martonchik, "Reflectance quantities in optical remote sensing-definitions and case studies," *Remote Sensing of Environment*, vol. 103, pp. 27–42, 2006.

[12] F. Gascon, C. Bouzinac, O. Thépaut, M. Jung, B. Francesconi, J. Louis, V. Lonjou, B. Lafrance, S. Massera, A. Gaudel-Vacaresse, and et al., "Copernicus sentinel-2a calibration and products validation status," *Remote Sensing*, vol. 9, no. 6, p. 584, Jun 2017. [Online]. Available: http://dx.doi.org/10.3390/rs9060584

[13] M. Weiss, F. Baret, and S. Jay, "S2toolbox level 2 products: Lai, fapar, fcover," Tech. Rep., 2020.

[14] F. J. García-Haro, M. Campos-Taberner, J. Muñoz-Marí, V. Laparra, F. Camacho, J. Sánchez-Zapero, and G. Camps-Valls, "Derivation of global vegetation biophysical parameters from eumetsat polar system," *ISPRS Journal of Photogrammetry and Remote Sensing*, vol. 139, pp. 57–74, 2018. [Online]. Available: https://www.sciencedirect.com/science/article/pii/S0924271618300625

[15] C. D. S. Copernicus Climate Change Service, "Leaf area index and fraction absorbed of photosynthetically active radiation 10-daily gridded data from 1981 to present," 2018.

[16] S. Blessing and R. Giering, "Algorithm theoretical basis document sentinel-3 cdr and icdr lai and fapar v4.0," Copernicus Climate Change Service, Tech. Rep., 2021.

[17] L. Graf, J. Gorroño, A. Hueni, A. Walter, and H. Aasen, "Propagating Sentinel-2 Top-of-Atmosphere Radiometric Uncertainty into Land Surface Phenology Metrics Using a Monte Carlo Framework," 3 2023. [Online]. Available: https://www.techrxiv.org/articles/preprint/Propagating_Sentinel-2_Top-of-Atmosphere_Radiometric_Uncertainty_into_Land_Surface_Phenology_Metrics_Using_a_Monte_Carlo_Framework/22179673

[18] M. Maahn, D. D. Turner, U. Löhnert, D. J. Posselt, K. Ebell, G. G. Mace, and J. M. Comstock, "Optimal estimation retrievals and their uncertainties: What every atmospheric scientist should know," *Bulletin of the American Meteorological Society*, vol. 101, no. 9, pp. E1512 – E1523, 2020. [Online]. Available: https://journals.ametsoc.org/view/journals/bams/101/9/bamsD190027.xml

[19] J. L. Widlowski, "Conformity testing of satellite-derived quantitative surface variables," *Environmental Science & Policy*, vol. 51, pp. 149–169, 2015.

[20] J. Louis, "Sentinel-2 level-2a algorithm theoretical basis document," 2021, available at https://sentinel.esa.int/web/sentinel/user-guides/sentinel-2-msi/document-library/-/asset_publisher/Wk0TKajiISaR/content/id/4363028, version 2.1.

[21] C. Emde, R. Buras-Schnell, A. Kylling, B. Mayer, J. Gasteiger, U. Hamann, J. Kylling, B. Richter, C. Pause, T. Dowling, and L. Bugliaro, "The libradtran software package for radiative transfer calculations (version 2.0.1)," *Geoscientific Model Development*, vol. 9, no. 5, pp. 1647–1672, 2016. [Online]. Available: https://gmd.copernicus.org/articles/9/1647/2016/

[22] B. Mayer and A. Kylling, "Technical note: The libradtran software package for radiative transfer calculations - description and examples of use," *Atmospheric Chemistry and Physics*, vol. 5, no. 7, pp. 1855–1877, 2005. [Online]. Available: https://acp.copernicus.org/articles/5/1855/2005/

[23] G. Thuillier, M. Hersé, D. Labs, T. Foujols, W. Peetermans, D. Gillotay, P. Simon, and H. Mandel, "The solar spectral irradiance from 200 to 2400 nm as measured by the solspec spectrometer from the atlas and eureca missions," *Solar Physics*, vol. 214, pp. 1–22, 05 2003.

[24] R. Richter and D. Schläpfer, "Atmospheric and topographic correction (atcor theoretical background document)," *DLR IB*, vol. 1, pp. 0564–03, 2019.

[25] J. Gorroño, S. Hunt, T. Scanlon, A. Banks, N. Fox, E. Woolliams, C. Underwood, F. Gascon, M. Peters, N. Fomferra, Y. Govaerts, N. Lamquin, and V. Bruniquel, "Providing uncertainty estimates of the sentinel-2 top-of-atmosphere measurements for radiometric validation activities," *European Journal of Remote Sensing*, vol. 51, no. 1, pp. 650–666, 2018.

[26] G. Thuillier, M. Hersé, P. Simon, D. Labs, H. Mandel, D. Gillotay, and T. Foujols, "The visible solar spectral irradiance from 350 to 850 nm as measured by the solspec spectrometer during the atlas i mission," *Solar Physics*, vol. 177, pp. 41–61, 01 1998.

[27] K. Stamnes, S.-C. Tsay, W. Wiscombe, and K. Jayaweera, "Numerically stable algorithm for discrete-ordinate-method radiative transfer in multiple scattering and emitting layered media," *Appl. Opt.*, vol. 27, no. 12, pp. 2502–2509, Jun 1988. [Online]. Available: https://opg.optica.org/ao/abstract.cfm?URI=ao-27-12-2502

[28] K. Stamnes, S.-C. Tsay, W. Wiscombe, and I. Laszlo, "Disort, a general-purpose fortran program for discrete-ordinate-method radiative transfer in scattering and emitting layered media: documentation of methodology," 2000.

[29] Y. Kaufman, A. Wald, L. Remer, B.-C. Gao, R.-R. Li, and L. Flynn, "The modis 2.1-/spl mu/m channel-correlation with visible reflectance for use in remote sensing of aerosol," *IEEE Transactions on Geoscience and Remote Sensing*, vol. 35, no. 5, pp. 1286–1298, 1997.

[30] J. Louis, B. Pflug, M. Main-Knorn, V. Debaecker, U. Mueller-Wilm, and F. Gascon, "Integration and assimilation of meteorological (ecmwf) aerosol estimates into sen2cor atmospheric correction," in *IGARSS 2018 - 2018 IEEE International Geoscience and Remote Sensing Symposium*, 2018, pp. 1894–1897.

[31] S2 MSI ESL team, "Sentinel 2 l2a data quality report," *Ref.: OMPC.CS.DQR.002.12-2022*, vol. 57, 2023, available at https://sentinel.esa.int/web/sentinel/technical-guides/sentinel-2-msi/data-quality-reports.

[32] JCGM, "Evaluation of measurement data - Guide to the expression of uncertainty in measurement," Tech. Rep. 100, 2008.

[33] D. Schläpfer, C. C. Borel, J. Keller, and K. I. Itten, "Atmospheric precorrected differential absorption technique to retrieve columnar water vapor," *Remote Sensing of Environment*, vol. 65, no. 3, pp. 353–366, 1998. [Online]. Available: https://www.sciencedirect.com/science/article/pii/S0034425798000443

[34] R. Dragani, "On the quality of the era-interim ozone reanalyses: comparisons with satellite data," *Quarterly Journal of the Royal Meteorological Society*, vol. 137, no. 658, pp. 1312–1326, 2011. [Online]. Available: https://rmets.onlinelibrary.wiley.com/doi/abs/10.1002/qj.821

[35] B. Hu, W. Lucht, and A. Strahler, "The interrelationship of atmospheric correction of reflectances and surface brdf retrieval: a sensitivity study," *IEEE Transactions on Geoscience and Remote Sensing*, vol. 37, no. 2, pp. 724–738, 1999.

[36] B. Franch, E. Vermote, J. Sobrino, and E. Fédèle, "Analysis of directional effects on atmospheric correction," *Remote Sensing of Environment*, vol. 128, pp. 276–288, 2013. [Online]. Available: https://www.sciencedirect.com/science/article/pii/S0034425712004063

[37] S. Y. Kotchenova, E. F. Vermote, R. Levy, and A. Lyapustin, "Radiative transfer codes for atmospheric correction and aerosol retrieval: intercomparison study," *Appl. Opt.*, vol. 47, no. 13, pp. 2215–2226, May 2008. [Online]. Available: https://opg.optica.org/ao/abstract.cfm?URI=ao-47-13-2215

[38] D. R. Thompson, N. Bohn, A. Braverman, P. G. Brodrick, N. Carmon, M. L. Eastwood, J. E. Fahlen, R. O. Green, M. C. Johnson, D. A. Roberts, and J. Susiluoto, "Scene invariants for quantifying radiative transfer uncertainty," *Remote Sensing of Environment*, vol. 260, p. 112432, 2021. [Online]. Available: https://www.sciencedirect.com/science/article/pii/S0034425721001504

[39] Y. Govaerts, Y. Nollet, and V. Leroy, "Radiative transfer model comparison with satellite observations over ceos calibration site libya-4," *Atmosphere*, vol. 13, no. 11, 2022. [Online]. Available: https://www.mdpi.com/2073-4433/13/11/1759

[40] J. Gasteiger, C. Emde, B. Mayer, R. Buras, S. Buehler, and O. Lemke, "Representative wavelengths absorption parameterization applied to satellite channels and spectral bands," *Journal of Quantitative Spectroscopy and Radiative Transfer*, vol. 148, pp. 99–115, 2014.

[Online]. Available: https://www.sciencedirect.com/science/article/pii/S0022407314002842

[41] E. Vermote, D. Tanré, J. Deuzé, M. Herman, J. Morcrette, and S. Kotchenova, "Second simulation of a satellite signal in the solar spectrum-vector (6sv)," *6S User Guide Version*, vol. 3, no. 2, pp. 1–55, 2006.

[42] J. Louis, V. Debaecker, B. Pflug, M. Main-Knorn, J. Bieniarz, U. Mueller-Wilm, E. Cadau, and F. Gascon, "Sentinel-2 sen2cor: L2a processor for users," in *ESA Living Planet Symposium 2016*, ser. ESA Special Publications (on CD), L. Ouwehand, Ed., vol. SP-740. Spacebooks Online, August 2016, pp. 1–8. [Online]. Available: https://elib.dlr.de/107381/

[43] S. Korkin, A. Sayer, A. Ibrahim, and A. Lyapustin, "A practical guide to writing a radiative transfer code," *Computer Physics Communications*, vol. 271, p. 108198, 2022. [Online]. Available: https://www.sciencedirect.com/science/article/pii/S0010465521003106

[44] M. G. Cox and B. R. L. Siebert, "The use of a Monte Carlo method for evaluating uncertainty and expanded uncertainty," *Metrologia*, vol. 43, no. 4, pp. S178–S188, Aug. 2006, publisher: IOP Publishing. [Online]. Available: https://doi.org/10.1088/0026-1394/43/4/s03

[45] JCGM, "Evaluation of measurement data — Supplement 1 to the "Guide to the expression of uncertainty in measurement" — Propagation of distributions using a Monte Carlo method," Tech. Rep. 101, 2008.

[46] H. Cosnefroy, M. Leroy, and X. Briottet, "Selection and characterization of saharan and arabian desert sites for the calibration of optical satellite sensors," *Remote Sensing of Environment*, vol. 58, no. 1, pp. 101–114, 1996. [Online]. Available: https://www.sciencedirect.com/science/article/pii/0034425795002111

[47] A. Toulemont, M. Olivier, S. Clerc, R. Bellouard, F. Reina, F. Gascon, J.-F. Luce, C. Mavrocordatos, and V. Boccia, "Copernicus Sentinel-2C/D Multi Spectral Instrument full field of view spectral characterization," in *Sensors, Systems, and Next-Generation Satellites XXV*, S. R. Babu, A. Hélière, and T. Kimura, Eds., vol. 11858, International Society for Optics and Photonics. SPIE, 2021, pp. 162 – 171. [Online]. Available: https://doi.org/10.1117/12.2593729

[48] J. Gorroño and L. Guanter, "Assessing the radiometric impact of the Sentinel 2 orthorectification process," in *Sensors, Systems, and Next-Generation Satellites XXV*, S. R. Babu, A. Hélière, and T. Kimura, Eds., vol. 11858, International Society for Optics and Photonics. SPIE, 2021, p. 118580W. [Online]. Available: https://doi.org/10.1117/12.2603730

[49] E. P. Shettle, "Models of aerosols, clouds, and precipitation for atmospheric propagation studies," 1990. [Online]. Available: https://api.semanticscholar.org/CorpusID:129735386

[50] C. D. S. Copernicus Climate Change Service, "Aerosol properties gridded data from 1995 to present derived from satellite observation. copernicus climate change service (c3s) climate data store (cds)," 2019.

[51] I. BIPM, I. IFCC, I. ISO, and O. IUPAP, "Evaluation of measurement data—supplement 2 to the 'guide to the expression of uncertainty in measurement'—extension to any number of output quantities," *JCGM*, vol. 102, p. 2011, 2011.

[52] M. Celesti, M. Rast, J. Adams, V. Boccia, F. Gascon, C. Isola, and J. Nieke, "The copernicus hyperspectral imaging mission for the environment (chime): Status and planning," in *IGARSS 2022 - 2022 IEEE International Geoscience and Remote Sensing Symposium*, 2022, pp. 5011–5014.

[53] J. Vicent, J. P. Rivera-Caicedo, J. Verrelst, J. Muñoz-Marí, N. Sabater, B. Berthelot, G. Camps-Valls, and J. Moreno, "Systematic assessment of modtran emulators for atmospheric correction," *IEEE Transactions on Geoscience and Remote Sensing*, pp. 1–17, 2021.

[54] P. G. Brodrick, D. R. Thompson, J. E. Fahlen, M. L. Eastwood, C. M. Sarture, S. R. Lundeen, W. Olson-Duvall, N. Carmon, and R. O. Green, "Generalized radiative transfer emulation for imaging spectroscopy reflectance retrievals," *Remote Sensing of Environment*, vol. 261, p. 112476, 2021. [Online]. Available: https://www.sciencedirect.com/science/article/pii/S0034425721001942

[55] C. D. Rodgers, *Inverse Methods for Atmospheric Sounding*. WORLD SCIENTIFIC, 2000. [Online]. Available: https://www.worldscientific.com/doi/abs/10.1142/3171

[56] F. Yin, P. E. Lewis, and J. L. Gómez-Dans, "Bayesian atmospheric correction over land: Sentinel-2/msi and landsat 8/oli," *Geoscientific Model Development*, vol. 15, no. 21, pp. 7933–7976, 2022. [Online]. Available: https://gmd.copernicus.org/articles/15/7933/2022/

[57] A. Braverman, J. Hobbs, J. Teixeira, and M. Gunson, "Post hoc uncertainty quantification for remote sensing observing systems," *SIAM/ASA Journal on Uncertainty Quantification*, vol. 9, no. 3, pp. 1064–1093, 2021. [Online]. Available: https://doi.org/10.1137/19M1304283

VII. BIOGRAPHY SECTION